Technological University Dublin

ARROW@TU Dublin

Articles

School of Electrical and Electronic Engineering

2017

Enhanced Network Voltage Management (NVM) Techniques Under the Proliferation of Rooftop Solar PV Installation in Low Voltage Distribution Network (LVDN)

Shivananda Pukhrem
Technological University Dublin

Malabika Basu
Technological University Dublin, mbasu@tudublin.ie

Michael Conlon
Technological University Dublin, michael.conlon@tudublin.ie

Keith Sunderland
Technological University Dublin, keith.sunderland@tudublin.ie

Follow this and additional works at: https://arrow.tudublin.ie/engscheleart2

Part of the Electrical and Computer Engineering Commons

Recommended Citation

Enhanced network voltage management techniques under the proliferation of rooftop solar PV installation in low voltage distribution network

Shivananda Pukhrem, Malabika Basu*, Michael Conlon and Keith Sunderland

Electrical Power Research Centre (EPRC)
School of Electrical and Electronic Engineering,
Dublin Institute of Technology,
Ireland

* corresponding author : mbasu@dit.ie

Abstract- **Proliferation of rooftop solar PV distributed generator (PVDG) installation in low voltage distribution network (LVDN) imposes voltage fluctuation challenges that are a threat to distribution system operators. Reactive power control (RPC) methods are insufficient in isolation to combat the overvoltage fluctuations manifested in LVDN with significant grid-tied PVDG installations. Whereas active power curtailment (APC) control can alleviate the voltage fluctuation in such situations and it is achieved at the cost of reduced active power injection. This paper explores how deficiencies in both RPC and APC as separate approaches can be mitigated by suitably combining RPC and APC algorithms. Strategies combining two RPCs and one RPC in conjunction with APC are proposed as two coordinating algorithms by means of instantaneous measurement of node voltage and active power. These coordinating algorithms are embedded in all the rooftop PVDG grid-tied-inverters (GTI), where the GTI coordinates among them for voltage support without exceeding individual inverter VA rating. The result of the combined approach show significant improvement in managing and stabilising the voltage and allows the penetration of PVDG to be increased from 35.65% to 66.7% of distribution transformer (DT) kVA rating.**

Keywords: distributed generation, network voltage management, reactive power control, active power curtailment, roof-top PV

I. INTRODUCTION

Solar PV distributed generator (PVDG) is considered an important role player to meet the renewable energy target in most of the countries [1]. However, the proliferation of rooftop solar PV distributed generator (PVDG) installation in low voltage distribution network (LVDN) imposes potential threats to distribution system operators (DSO) as it facilitates bi-directional power flow [2, 3, 4, 5]. Intermittent power output and placement of the PVDG sources on distribution feeder can create voltage control issues on traditional voltage regulators and on load tap changer transformers. The normal operation of devices such as on load tap changers (OLTC), line voltage regulators (LVR), capacitor switch banks (CSB), line drop compensators (LDC), switchgear and protection systems (SGP), relays (R) and other ancillary devices are mostly unidirectional. The operation of these devices may be affected as a consequence of the reverse power flow provided by distribution network with significant PVDG connection. Such reverse power flow is due to the voltage rise at the far end of the LVDN feeder [6, 7, 8]. Voltage rise in such context occurs when the injected PVDG current is higher than the upstream current [9]. Figure1 (a) illustrates a typical phenomenon when a significant amount of PVDGs are installed at unity power factor (i.e. $\Phi = 0°$, where Φ is the phase angle between current and voltage at the point of connection of PVDG) for a typical radial feeder with an impedance phase angle of φ (where φ is the phase angle between resistive and reactive component of the line). Therein, voltage rise is realized due to $I_{PVDG} > I_{LINE}$ where, I_{PVDG} is the current flowing from the installed PVDG and I_{LINE} is current flowing through

1

the line. With respect to Figure 1(a), E represents the voltage at the upstream node, V_{POC} is a representation of the voltage at the POC (Point Of Connection) where PDVG is installed, R is line resistance, X is line reactance, I_F is forward current ($I_{LINE} - I_{PVDG} > 0$) , I_R is reverse current ($I_{LINE} - I_{PVDG} < 0$) and V_{DROP} represents the voltage dropped in the line.
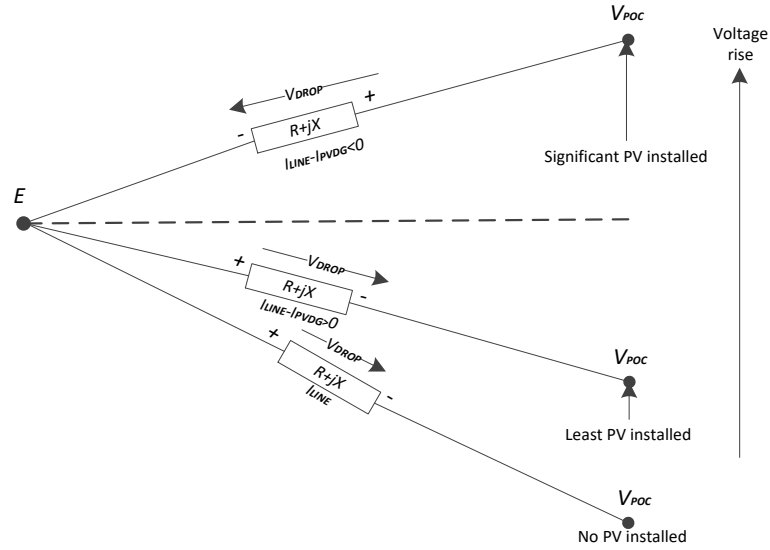

Figure 1(a): Illustration of flow of power during significant PVDG installed at V_{POC} [9]

This typical phenomenon can be studied using a phasor representation of Figure 1(a) which is illustrated in Figure 1(b). Here E is considered as a reference point of our phasor illustration. Let us assume that PVDG is injecting current (I_{PVDG}) into the line at a phase lead of an angle δ from the reference point E. Moreover from earlier discussion, PVDG is injecting power at unity power factor, which means I_{PVDG} is in phase with V_{POC} i.e. Φ =0°.Correspondingly, V_{R_LINE} (the voltage drop in the resistive component of the line) is plotted in phase with I_{PVDG}.Subsequently, V_{X_LINE} (the voltage drop across the reactive component of the line) is also plotted orthogonal to V_{R_LINE}. The resultant phasor V_{DROP} is the vector sum of V_{R_LINE} and V_{X_LINE}. The angle between V_{R_LINE} and V_{X_LINE} is also the impedance phase angle φ. Finally, the voltage at the point of connection V_{POC} is obtained as a resultant vector sum of E and V_{DROP} i.e. in magnitude, $|V_{POC}| = \{|E| + |V_{DROP}\cos(\delta + \varphi)|\}$. The angle δ is also the phase voltage difference between phasors V_{POC} and E. It is clear in Figure 1(b) that $|V_{POC}| > |E|$ due to PVDG integration. If significant PVDG are installed, this voltage rise phenomena will aggregate and will be highest at the end of the feeder.
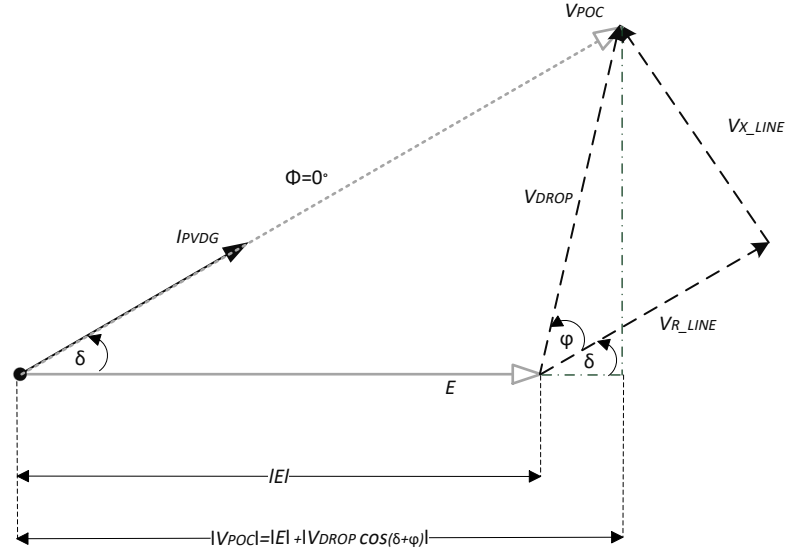
A further consequence of resultant reverse power flow is that it could also increase the loading at the upstream transformer and thereby restrict the PVDG penetration level in the LVDN. Authors in [10], applied an impedance monitoring method for detecting the current distribution system state in which PVDG penetration level can be observed to monitor its reverse power flow.

Traditional voltage fluctuation control devices such as OLTC, LVR and CSB are not primarily designed to mitigate the fluctuations in voltage caused by the intermittent primary energy resource (solar insolation) [9, 11]. Nonetheless, as discussed by Yashodhan *et al.*in [12], an optimal reactive power coordination strategy based on the load and irradiance forecast data can be employed to reduce the duty associated with the operation of OLTC and LVR. Furthermore, as proposed by Jung *et al.* [13], coordinating techniques can be deployed to overcome voltage fluctuations through the synergetic operation of automated voltage regulators and capacitors in conjunction with PVDG inverters. Flexible AC transmission system (FACTS) devices can also alleviate operational frequency of these devices. Zhang *et al*. in [14] deployed dynamic VAR compensation to mitigate the voltage fluctuations. Reduced frequency operation of OLTC, LVR, and CSB without the support of FACTS devices, can be supplemented through smart functionality on the PVDG grid-tied-inverter (GTI) to alleviate the voltage fluctuation. Such smart functionality of the GTI monitors the voltage within its vicinity and responds to an appropriate VAR requirement by the distribution network [15]. With the advanced control capability of smart GTI [16], which essentially has FACTS functionality to a limited extent, the requirement of additional devices is eliminated and the uncertainty error caused by irradiance and load forecast, as discussed earlier, is much less influential.

So far, reactive power control (RPC) methods include Q (U) control (reactive power as a function of the local voltage), PF (P) control (power factor as a function of the PVDG active power) and PF (U) control (power factor as a function of the local voltage). Whereas, an active power curtailment (APC) method is P (U) control (active power as a function of the local voltage). The VAR management for alleviating the voltage fluctuation depends primarily on

the VA capacity of the PVDG GTI, upstream transformer loading, and any associated line and transformer losses. From a European perspective, German grid code as discussed in [17] and [18] respectively, recommends the active involvement of PVDG GTI to alleviate the voltage fluctuation at the point of connection as a technical requirement for the connection to MV and LV networks.

A further alternative to the German grid code is a technique proposed in [19] that alleviates voltage fluctuation for a LV balanced network by controlling the power factor (PF) of the GTI through continuous monitoring of active PVDG power (P) and the voltage (U) within its vicinity (PF(P,U)). On the other hand, this approach imposes higher upstream transformer loading when compared with the other techniques cited in [19] such as Q (U) and PF (P). Normally, the P (U) control is limited by the VA rating of the PVDG GTI; however, in reality, the PVDG output power fluctuates and could exceed its VA rating. According to Collins and Ward in [20], instantaneous fluctuating PVDG power can be employed to monitor the VA rating of PVDG GTI by utilizing dynamic maximum reference as a control technique for P (U) control along with the Q (U) to alleviate the voltage fluctuation for the Australian long rural MV feeder network. Nevertheless, such an approach comes with higher curtailment losses, which must be considered, even if the methodology performs well in alleviating resultant voltage fluctuations. In other work, a local linear control is investigated to substitute the real power into reactive power when the output power fluctuates thereby mitigating any voltage fluctuation [21]. There, the authors investigated methods of selecting the control parameter through sensitivity minimization and violation optimization. The limitation of such an approach is that there is no valid result if the number of buses in the distribution system is large (i.e. more than five buses).

In a typical European low voltage (LV) distribution network (three-phase four-wire), the conglomeration connection of single-phase PVDG system (mostly rooftop) and different loads could create an unbalance in the LVDN. This is mainly due to a neutral point shifting of the three-phase voltages occurring while injecting active power and injecting or absorbing reactive power by the PVDG inverter. Exploiting the RPCs in such unbalanced network is challenging, yet Weck *et al.* in [22] suggested that by tuning the control parameters optimally, which are grid and time dependent, the local controllers of active and reactive power could potentially reduce the voltage fluctuation without shifting the neutral point of the three-phase voltage. This was achieved by optimal injection or absorption of reactive power in one phase to avoid excessive voltage in other phases. Moreover, as described in [23], the operation of Q (U) control, in conjunction with the injection of correction current, mitigates the voltage fluctuation and reconfigures the unbalanced network to a balanced network. Therein, both single phase and three phase inverters are used to achieve this approach. Thus, voltage unbalance mitigation procedure in conjunction with the operation of the RPC techniques is equally important to alleviate the voltage fluctuation.

Practical implementation of voltage management control has great influence in designing any RPCs or APC. In [24], the authors consider two systems for implementing Q (U) control techniques digitally, namely, discrete-time system and discrete-time dynamic system (resembles continuous-time response system). Herein, the stability of implementing each control technique was performed and it was concluded that implementation of the discrete-time dynamic system is asymptotically stable when compared to the simple discrete-time system. But the analysis performed in [24] shows that instability occurs due to delay measurement in the Q (U) control loop. Andrén et al. in

[25] performed a comprehensive study on the stability analysis of Q (U) voltage control in PV single inverter and multi-inverter integration in a low voltage distribution network. In this case, the system stability was based on three parameters such as open loop gain of the Q (U) control technique, Q (U) control time response and time delay which is the sum of delays in the controller loop. Based on these parametric values, stability Q (U) can be achieved only when the geometric distance between total delay and Q (U) controller time response is higher in proportionate to higher open loop gain (i.e. large network reactance, high inverter and high droop factor).Moreover, from [25], instability has been observed to be based on the total time-delay in numerical simulation. An interesting aspect of the stability analysis of real word implementation of Q (U) and P (U) controllers is discussed in [26]. Here, the authors point out that, the dynamic behaviour of the voltage at the point of connection (E) under the required reactive power (Q) for Q (U) control, has a unique equilibrium point. In this regard, the local stability of the equilibrium point of E may be determined by calculating the magnitude of E's Jacobian at that equilibrium point. Depending on this magnitude, stability of the operation between Q (U) and P (U) was performed. It was concluded that instability in such operation could arise as a function of design parameters such as measurement filter design, Q (U) and P (U) functions to design and consideration of specific operating condition. Furthermore, Liu et al. in [27] proposed a method to analyze the dynamic stability of power systems under the influence of RPCs for voltage control due to a stochastic characteristic of PV power generation. There, the authors introduced a probabilistic small signal stability analysis method which depends on grid parameters, gains of the constant dc voltage controller and joint variation of the gain pair of the current controller in d-axis.

PF (P) control is implemented as a function of PVDG active power which depends on irradiance and temperature. Whenever high irradiance coincides with high peak demand, the voltage rise may not exceed the overvoltage limitation and the requirement of such a technique will be unnecessary. Furthermore, it regulates all the PVDG GTI participating in the public network irrespective of the voltage profile. The Q (U) controller on the other hand exchanges reactive power when the solar PVDG sources are not the primary source of the voltage fluctuation. Although, this method directly uses the instantaneous information of the local voltage which is a consequence of the PVDG power production and the activity of the load demand is in its vicinity. Again, Q (U) control may not react to critical voltage fluctuation at the far end feeder when it is embedded to the rooftop PVDG GTI located near the distribution transformer (DT). Furthermore, PF (U) controller also exchanges reactive power when the solar PVDG source is generating active power. In [28], a stable operation of PF (U) is evaluated in solar PV inverter. However, the droop control of PF (U) and Q (U) are different as the former uses power factor and the latter uses reactive power. But under equal grid impedances and generation of active power, the two functions can be made to generate an equal amount of reactive power. Samadi et al.in [29] also evaluated the different technical aspect of recent German grid code called an active power dependent standard characteristic curve, Q (P). There, the authors utilize voltage sensitivity matrix to calculate the exact required reactive power in each node. A strategy to support grid stability in the event of frequency-voltage variation was reported in [30]. Here, the authors considered electrical energy storage to extend the existing standards for grid support. However, the authors have not discussed the extended grid support under internode activity and contingency disturbances at distribution system level.

5

However, if combinations of coordinating algorithms among the existing voltage control techniques are of any additional advantage has not been addressed in detail [19, 20]. The objective of this paper is to enhance PVDG penetration by combating critical voltage fluctuation with the help of combining a few coordinating algorithms. The importance of this paper lies in implementing two different algorithms in a real suburban Dublin LVDN without exceeding the VA rating of the converters. Power factor (PF), node voltage (U) and active power (P) are the three critical informations for each of the nodes. No communications between nodes are necessary.

Here, GTIs closer to DT have PF closer to unity power factor (UPF) while GTIs near the far end has PF closer to ±0.90 depending on the voltage profile. Then, power flow is calculated in terms of increasing PVDG penetration (see Appendix 1 subsection 1 for the associated rationale). The voltage fluctuation profile is observed subsequently when all the GTIs are equipped with 3 different RPCs namely Q(U), PF(P) and PF(U) and the two proposed coordinating algorithms namely Q(U) & P(U) and PF(U) & PF(P).

Through these two co-ordinating algorithms, the voltages in each node were maintained and stabilised within the limit by minimizing the system losses and transformer loading. Additionally, this paper also highlights a new concept of implementing smoother RPC and APC droop function. The unwanted inherent oscillating behaviour of the operating point in the two proposed coordinating algorithms is arrested by designing a novel 'Q' or 'PF' limiter which helps to stabilise the voltage without violating the maximum limit. Such oscillating behaviour of the operating point arises due to the frequent switching requirement between two droop functions which is dependent on the present value of U.

The paper is sectionalized as follows. The first section briefly describes the specification of the considered LVDN along with the summary on voltage fluctuation management and impedance based stability. The second section summarizes the development of coordination algorithms which allows PVDG penetration to be increased from 35.65 % to 66.70% of DT kVA rating. The third section presents a thorough discussion of the comparative studies and results based on the different approaches to combat the voltage fluctuation concerns. Finally, the fourth and final part of the paper presents the conclusions and suggestions for future work.

II. NETWORK SPECIFICATION AND MANAGEMENT OF VOLTAGE FLUCTUATION

A. Network Specification

As illustrated in Figure 2, the considered layout comprises a part of low voltage (LV) urban distribution network consisting of 74 single phase domestic homes supplied by 9 pillars (designated alphabetically) through a 20kV/400V supply. A source impedance of 23.094 Ω (which corresponds to fault current level of 0.5 kA see Appendix 1 subsection 2) is added to the source bus which is the high voltage (20kV) side of the two windings star-star(y-y) connected transformer. The rating of this transformer is 500 KVA and 20kV/400V with 10% of reactance from winding 1 (high) to winding 2 (low) and 0.4% of load losses(see Appendix 1 subsection 3 for the rationale). The considered network is modeled as a radial feeder in a structure in which the network sub-feeder cables (inter-node connections) modeled as overhead cables. The sub-feeder cables (X/R>1) are 120mm^2 and 70mm^2, with copper conductors and cross-linked polyethylene insulation (XLPE) with some connections facilitated by 70mm^2 cables with aluminum conductors; also

6

XLPE insulated. The node to consumer connections is facilitated through 25mm^2 concentric neutral cable, with polyvinyl chloride (PVC) insulation ($X/R<1$). The detailed modeling of the considered LV radial distribution network is described in [31]. Out of 74 residents, 31 are assigned a single phase PVDG generator with the maximum allowed individual peak power ratings (kW_p) of 5.75 kW [32]. Both PVDG and load demand are modeled as a purely active power component. The detailed distribution of the peak load demand and 31 customer PVDG installations for the considered network are shown in Figure 2 where node 73rd is the last node to install PVDG. Table I summarizes the load and PVDG distributions where two types of PVDG penetration scenarios are considered, namely with 31 and 58 PVDG installations, which represents a penetration level of 35.65 % and 66.70% of the DT kVA rating respectively (see Appendix 1 for the associated rationale).
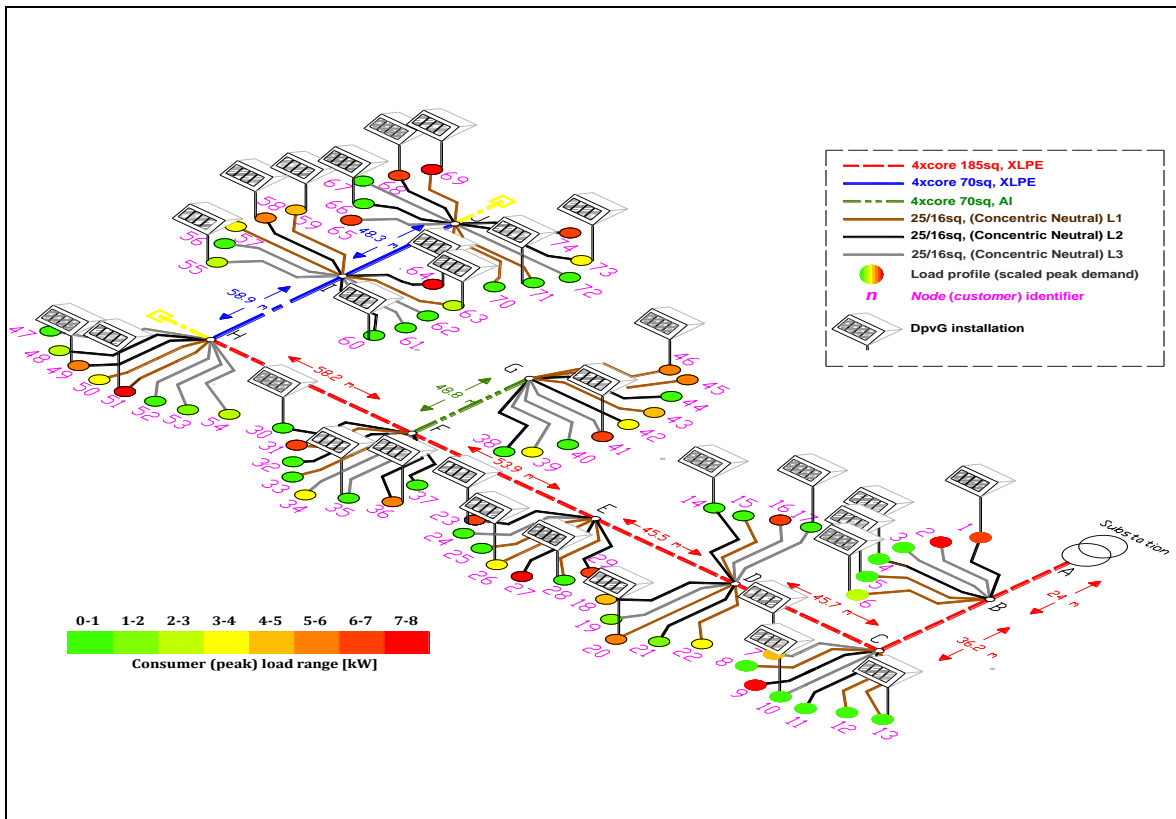

Figure 2: LVDN illustrating the connection of rooftop 31 PVDGs installation

TABLE I

CUSTOMER PEAK LOAD DEMAND AND PVDGS INSTALLATION DISTRIBUTION

Peak load distribution in kW	% of customer connecting the load (out of 74)	% of customer installing PVDG (out of 31)	% of customer installing PVDG (out of 58)
$0< \text{Peak}_{\text{load demand}} <1$	47.3	48.39%	39.66%
$1< \text{Peak}_{\text{load demand}} <6$	33.8	29.03%	37.93%
$\text{Peak}_{\text{load demand}} \geq 6$	18.9	22.58%	22.41%

B. Recorded PVDG and Load data

For the LVDN considered here, it is assumed that all 74 residents receive the same solar irradiance. The solar irradiance recorded by the Whitworth Meteorological Observatory in Manchester, UK [33] in 2013 is considered as the representative of solar resource for the network illustrated in Figure 2. The irradiance observed from meteorological data is transformed into single phase PVDG generator profiles with the efficiencies of 15 % and 95 % for the energy conversion process and the inverter respectively, as described in [34].The typical single phase domestic customer PVDG generator and load profile data having a resolution of 5 minutes was acquired from [35]. Figure 3 illustrates both load and PVDG profiles. The PVDG output is considered over the course of a single day. Again it is assumed that all the 74 residents have similar residential load profiles representative of typical single phase domestic customers with different peak demands.
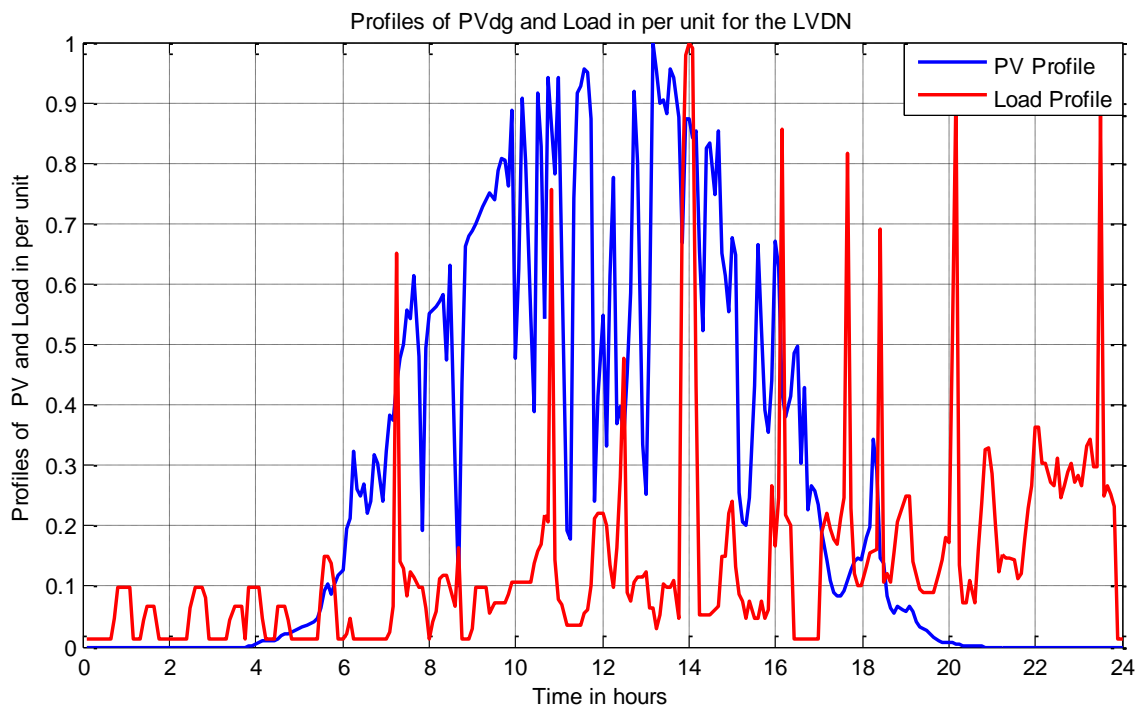

Figure 3: Recorded PVDG and Load profile in per unit

C. Voltage fluctuation management

Referring to Figure 4, whenever a PVDG source exports power, it operates between quadrant 2 and 3 of the four quadrant representation of GTI active and reactive power. Quadrant 2 represents an injection of reactive power (equivalent to the capacitive element) and quadrant 3 represents absorption of reactive power (equivalent to the inductive element). Within quadrants 2 and 3, RPC regulates the PVDG phase angle from 90^0 to 270^0 to exchange the required reactive power (i.e. vertical axis of the four quadrants) of the GTI in order to combat any voltage fluctuation. Whereas in the case of APC , the horizontal axis (i.e. active power) of the four quadrants can control the absolute magnitude of the active power to reduce its injection into the LVDN; thereby alleviating the critical voltage

8

fluctuation. In the case of under voltage, the GTI can overexcite to inject reactive power until it hits the rated VA limit by shifting the PVDG phase angle towards + Var, i.e. towards 90°. Whereas, with over voltage the GTI can under excite to absorb reactive power until it reaches the rated VA limit by shifting the PVDG phase angle towards –Var, i.e. towards 270°. Recently, most of the PVDG GTI is configured to increase its VA rating to accommodate better voltage support. In the following section of this paper, optimal exploitation of active and reactive power control for voltage fluctuation management in LVDN is considered.
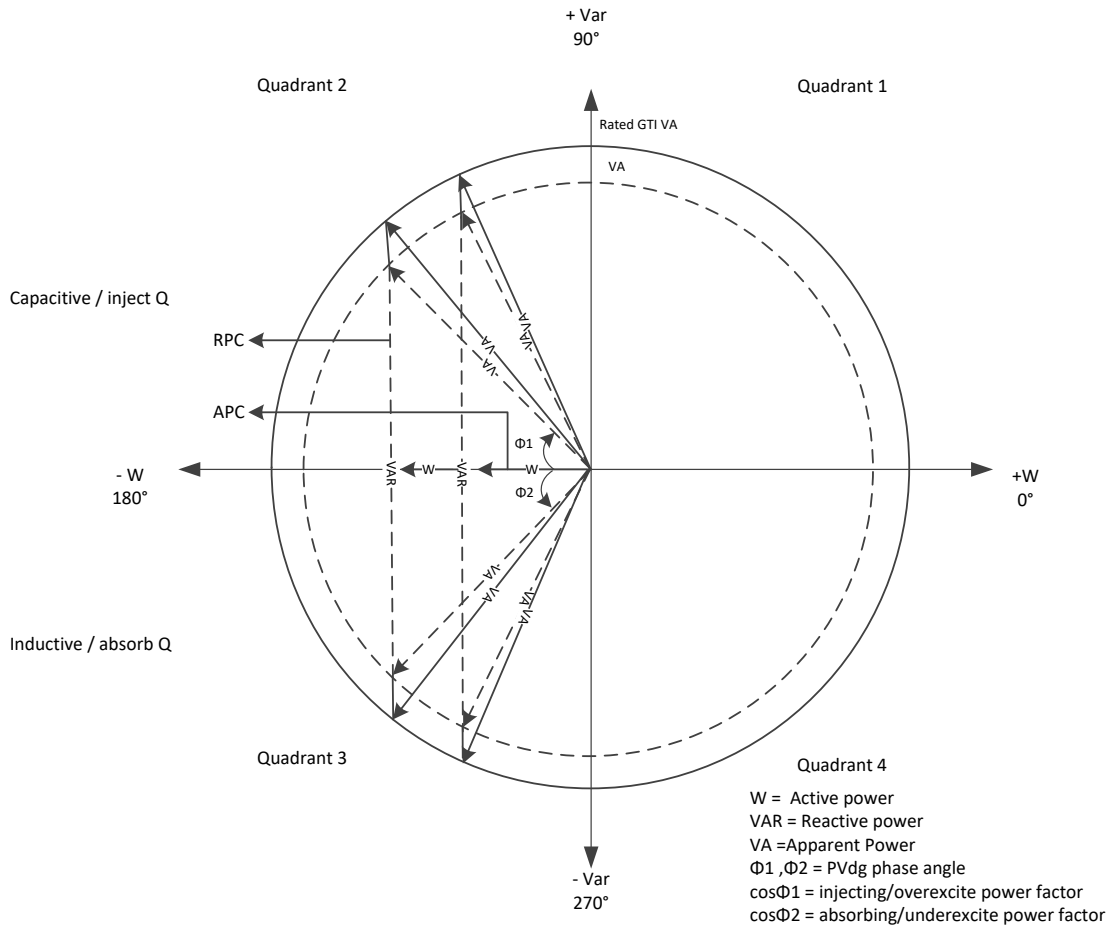

Figure 4: Four quadrant representation of active/reactive in GTI

D. Impedance based stability issues

Before going to the details of the coordinated voltage management issues, it would be important to highlight some aspects of real field implementation challenges with power electronic interface that would govern the success of system level voltage coordination and regulation within the limit. The effects of voltage variation on system stability are profoundly influenced by the connecting filters that are likely to interact with the grid impedances typically in a weak distribution network [36, 37, 38].

Being aware of the problem the researchers have taken appropriate measures through design and control actions. It is very important that the farthest point of PV injection into the radial network would operate with sufficient phase

9

margin to ensure system-level stability. Among various methods the impedance based small signal analysis is quite useful in deriving the stability [39, 40].This literature also provides a Return Ratio Matrix (RRM) [41] method that would help to determine the overall stability of the system based on zero or non-zero encirclement of the characteristic loci around (-1, j0) point. This design will also be influenced by the possible grid impedance variation that will affect input and output impedances, filter resonant frequencies [42, 43, 44] and the system stability can be evaluated by Nyquist stability criteria [45, 46, 47, 48]. Therefore, the impact of the change in the operating point has to be evaluated for the worst possible case scenario stability assessment. This would mean considering the variation in output current and voltage phase angle variation would impact the admittance of the network at a particular point. A good power electronic based design will ensure that low-frequency disturbances are within the designed controller bandwidth (e.g. PLL and outer power loop bandwidth etc.). When the harmonic stability is of concern, the design of inner current control loop is of critical importance [44, 47, 49, 50, 51, 52].In the present paper, further discussion is restricted as the focus is on system level voltage regulation with novel coordinating algorithms.

III. COORDINATION ALGORITHMS AND RESULTS

A. Reactive Power Control (RPCs)

To achieve higher penetrations of rooftop PVDG in LVDN, without violating any voltage fluctuation (as per *EN 50438 [53]* requirements i.e. $\pm 10\%$ $U_{Nominal}$ of 230 V), synergetic coordination of all the installed PVDG GTI is important. This is achieved through embedding coordination algorithms. RPCs are widely adopted for voltage fluctuation problems, however, due to the limitation of VA rating, VAR usage is also limited to PF = ± 0.90. Table II presents different RPCs with their corresponding droop curves, equations, and droop parameters. For each RPCs, the VAR usage is limited to PF = - 0.90.

TABLE II

DIFFERENT TECHNIQUES AND THEIR CORRESPONDING DROOP CHARACTERISTICS

Techniques	Droop curve	Droop Equations	Droop parameters
Q(U)		$Q(U)$ $= \begin{cases} Q_2 & , U \leq U_1 \\ Q_2 + (Q_{max} - Q_2)\left(\dfrac{U - U_1}{U_2 - U_1}\right) & , U_1 < U \leq U_2 \\ Q_{max} & , U > U_2 \end{cases}$	$Q_{max} = -P_n \sqrt{\dfrac{1}{(cos\Phi)^2} - 1}$ $cos\Phi = [0.9]$ lagging $Q_2 = 0$ $U_1 = 1.05$ $U_2 = 1.1$ Where ,$P_n = 5.75$ kW

PF(P)		$PF(P)$ $= \begin{cases} 1 & ,P \leq P_1 \\ -1 + (cos\Phi + 1)\left(\dfrac{P - P_1}{P_2 - P_1}\right) & , P_1 < P \leq P_2 \\ cos\Phi & , P > P_2 \end{cases}$	$cos\Phi = [0.9]$ lagging $P_1 = 0.5$ $P_2 = 1$
PF(U)		$P(U)$ $= \begin{cases} 1 & ,U \leq U_1 \\ -1 + (cos\Phi + 1)\left(\dfrac{U - U_1}{U_2 - U_1}\right) & , U_1 < U \leq U_2 \\ cos\Phi & , U > U_2 \end{cases}$	$cos\Phi = [0.9]$ lagging $U_1 = 1.05$ $U_2 = 1.1$

B. Design of Coordinating Algorithms

Whenever any node voltage in LVDN exceeds the critical voltage limit i.e.1.1 p.u and simultaneously the VAR usages are exhausted, the coordinating algorithms extend the voltage support controllability of each of the PV GTIs. The first coordinating algorithm combines two RPCs namely, PF (U) and PF (P). As discussed earlier in the introduction, PF (U) is a function of instantaneous node voltage and can only support voltage until the GTI VA rating is reached. GTIs closer to DT are unable to support voltage fluctuation at the far end when it is embedded with PF (U). In such cases, another RPC such as PF (P) could be effective as it can regulate all the GTIs in the LVDN irrespective of the nodal voltages. The procedure for such coordinating algorithm is as follows. Initially, all PV GTIs are embedded with PF (U) where it maintains the voltage support mechanism up to the PV GTI VA rating. Once any node voltages exceed the first voltage limit (1.08p.u) and simultaneously the VAR option is exhausted, the voltage support technique will switch from PF (U) to PF (P). Subsequently, the corresponding required *PF (Ux)* for such node voltage (> 1.08 p.u) is calculated using the droop curve, equations, and parameters as given in Table III. Using this new *PF (Ux)* as one of the droop parameters, the voltage support technique switches to PF (P) where it controls the PF of all PV GTIs irrespective of the voltage information. Moreover, when the node voltage is less than 1.08 p.u, the voltage support technique reverts back to PF (U) from PF (P). Thus, through such coordinating technique the voltage support in LVDN can be achieved when the PV penetration increases.

Techniques	Droop curve	Droop Equations	Droop parameters
PF(U) & PF(P)	*(droop curves: U/Un vs cosφ and P/Pn vs cosφ; PF Lagging, Underexcite/ Overvoltage, Towards Distribution transformer)*	$PF(U,P)$ $$=\begin{cases} cos\Phi_{UPF} & , U \le U_1 \\ -1 + (cos\Phi + 1)\left(\frac{U-U_1}{U_2-U_1}\right) & , U_1 < U \le U_2 \\ PF(Ux) = -1 + (cos\Phi+1)\left(\frac{U-U_1}{U_3-U_1}\right) & , U > U_2 \\ -1 + (PF(Ux)+1)\left(\frac{P-P_1}{P_2-P_1}\right), P_1 \le U \le P_2 \\ cos\Phi & , U > U_3 \end{cases}$$	$U_1 = 1.04$ $U_2 = 1.08$ $U_3 = 1.1$ $P_1 = 1$ $P_2 = 0.5$ $cos\Phi = [0.9]$ lagging $cos\Phi_{UPF} = 1$
Q(U) & P(U)	*(droop curves: U/Un vs Q and P/Pn; $\sqrt{S^2 - Q^{*2}}$; Underexcite/ Overvoltage, Towards Distribution transformer)*	$Q(U) = \begin{cases} Q_2 & , U \le U_1 \\ Q_3 = \left[Q_2 + (Q_1 - Q)\left(\frac{U-U_1}{U_2-U_1}\right)\right] & , U_1 < U \le U_2 , U > \\ \text{Change the droop curve to } P(U) & U_2 \end{cases}$ $P(U) = \begin{cases} Q^* = Q_2 + (U-U_1)\left(\frac{Q_1-Q_2}{U_3-U_1}\right) \\ P^* = \sqrt{S^2 - Q^{*2}} & , U > U_2 \\ P_1 + (U-U_1)\left(\frac{P^*-P_1}{U_3-U_1}\right) & , U_1 \le U \le U_3 \\ P^* & , U > U_3 \end{cases}$	Q_1 $= -Pn\sqrt{\frac{1}{(cos\Phi)^2} - 1}$ $Q_2 = 0$ $U_1 = 1.04$ $U_2 = 1.08$, $U_3 = 1.1$ $P_1 = 1$ $cos\Phi = [0.9]$ lagging

The second coordinating algorithm works in a similar manner, but it combines one RPC namely, Q (U) and one APC, namely P (U). As mentioned earlier in the introduction part, Q (U) could be inefficient as voltage support mechanism for the far-end node when the VAR exchange is restricted to the VA rating. Therefore, APC such as P (U) could assist in voltage support in a similar situation. The procedure for the analogous coordinating algorithm is as follows. All the PV GTIs are embedded with Q (U) at the beginning. When any node voltages exceed the first voltage limit (1.08p.u) and simultaneously the VAR support is exhausted, the voltage support technique will switch from Q (U) to P (U). Furthermore, the corresponding Q^* to support the voltage when the node voltage is greater than 1.08 p.u is calculated using the droop curve, equations, and parameters as given in Table III. Using this new Q^*, the corresponding P^* is calculated and assigned as one of the droop parameters for the voltage support technique P (U) where it controls the active power (P) of all PV GTI in terms of the instantaneous voltage information. Additionally, once the node voltage is less than 1.08 p.u, the voltage support technique will revert back to Q (U) from P (U).Thus, through such a coordinating technique, equivalent LVDN voltage support is achievable by assigning the required Q^* for voltage support and thereby curtailing the minimum required P. Hence through these two coordinating algorithms, effective voltage support can be achieved by overcoming each individual controllability limitation.

The procedure to execute voltage management technique in LVDN is as follows. Initially, all the LVDN parameters (line parameters, the distance between each node and buses, bus data information), PVDG and load profiles are accumulated to perform a quasi-time series power flow analysis using OpenDSS [54] for every 5 minutes. The implementation of power flow in a co-simulation platform between MATLAB and OpenDSS is discussed in [55]. As

mentioned before in section II subsection B, all the PVDG and load demand are equipped with UPF. The power flow will stop only when the total time reaches 1440 minutes which corresponds to 24 hours. For every 5 minute time step, the instantaneous voltage profile at each of the PVDG installed nodes (node 'p') are monitored '$(V_{t_n})_p$' where 'p' denote a particular PV installed node and 't_n' is the instantaneous time. If $(V_{t_n})_p \leq V_j$ is satisfied where V_j =1.04 p.u, each PVDG GTIs will stay in idle stage i.e. their PF will be UPF. Otherwise, if $V_j < (V_{t_n})_p \leq V_k$ is satisfied where $V_k = 1.08$ p.u, then 'Q' or 'PF' limiter algorithm is activated. 'Q' or 'PF' limiter algorithm is given in steps a-e. Due to rapid fluctuation of irradiance, 'Q' or 'PF' limiter algorithm is necessary to mitigate frequent switching between two droop characteristics.

 a. Compute the static 'Q' or 'PF' from the droop characteristics from Table III.

 b. Find the absolute difference between the previous i.e. $(Q_{t_{n-1}})_p$ or $(PF_{t_{n-1}})_p$ and present i.e. $(Q_{t_n})_p$

  or $(PF_{t_n})_p$ values of 'Q' or 'PF'. In other words, $\Delta Q = \left|(Q_{t_n})_p - (Q_{t_{n-1}})_p\right|$ or $\Delta PF = \left|(PF_{t_n})_p - (PF_{t_{n-1}})_p\right|$.

 c. If both $(V_{t_n})_p > (V_{t_{n-1}})_p$ i.e. difference between the present and past instantaneous node voltage and $\Delta Q < \varepsilon_1$ or $\Delta PF < \varepsilon_2$ conditions are simultaneously satisfied, then assign the new required 'Q' or 'PF' as the present static value calculated from the droop equation.

 d. If $(V_{t_n})_p > (V_{t_{n-1}})_p$ is satisfied and $\Delta Q < \varepsilon_1$ or $\Delta PF < \varepsilon_2$ is not satisfied, then the required 'Q' or 'PF' is calculated as follows: $(Q_{t_n})_p = (Q_{t_{n-1}})_p + \Delta Q/\delta$ or $(PF_{t_n})_p = (PF_{t_{n-1}})_p + \Delta PF/\delta$.

 e. However, if $(V_{t_n})_p > (V_{t_{n-1}})_p$ is not satisfied then, the required 'Q' or 'PF' is calculated as follows: $(Q_{t_n})_p = (Q_{t_{n-1}})_p$ or $(PF_{t_n})_p = (PF_{t_{n-1}})_p$.

After 'Q' or 'PF' limiter algorithm is activated, the required 'Q' or 'PF' for Q (U) or PF (U) voltage control is assigned to all the PVDG GTI without exceeding VA rating of the GTIs. However, if $V_j < (V_{t_n})_p \leq V_k$ is not satisfied and simultaneously $(V_{t_n})_p > V_k$ is satisfied then 'Q' or 'PF' limiter algorithm is activated thereby computing necessary corresponding *PF (Ux)* or Q^* from the $(V_{t_n})_p$ as the extreme measure. Subsequently, the droop characteristic changes from Q (U) to P (U) or PF (U) to PF (P). Finally, depending on $(V_{t_n})_p$ value if $V_j < (V_{t_n})_p \leq V_k$ is satisfied, the droop characteristic reverts back from P (U) to Q (U) or PF (P) to PF (U) only after passing through 'Q' or 'PF' limiter . The process is continued until the simulation time (1440 minutes) is over for the entire PV installed node. The entire flow of the process is shown as a flowchart in Figure 5. In the following part of this paper, different RPCs and two coordinating algorithms are simulated to validate their performance. Herein, $\varepsilon_1, \varepsilon_2$ and δ are obtained after heuristic method. These values have a direct influence on the performance of the network voltage management control.
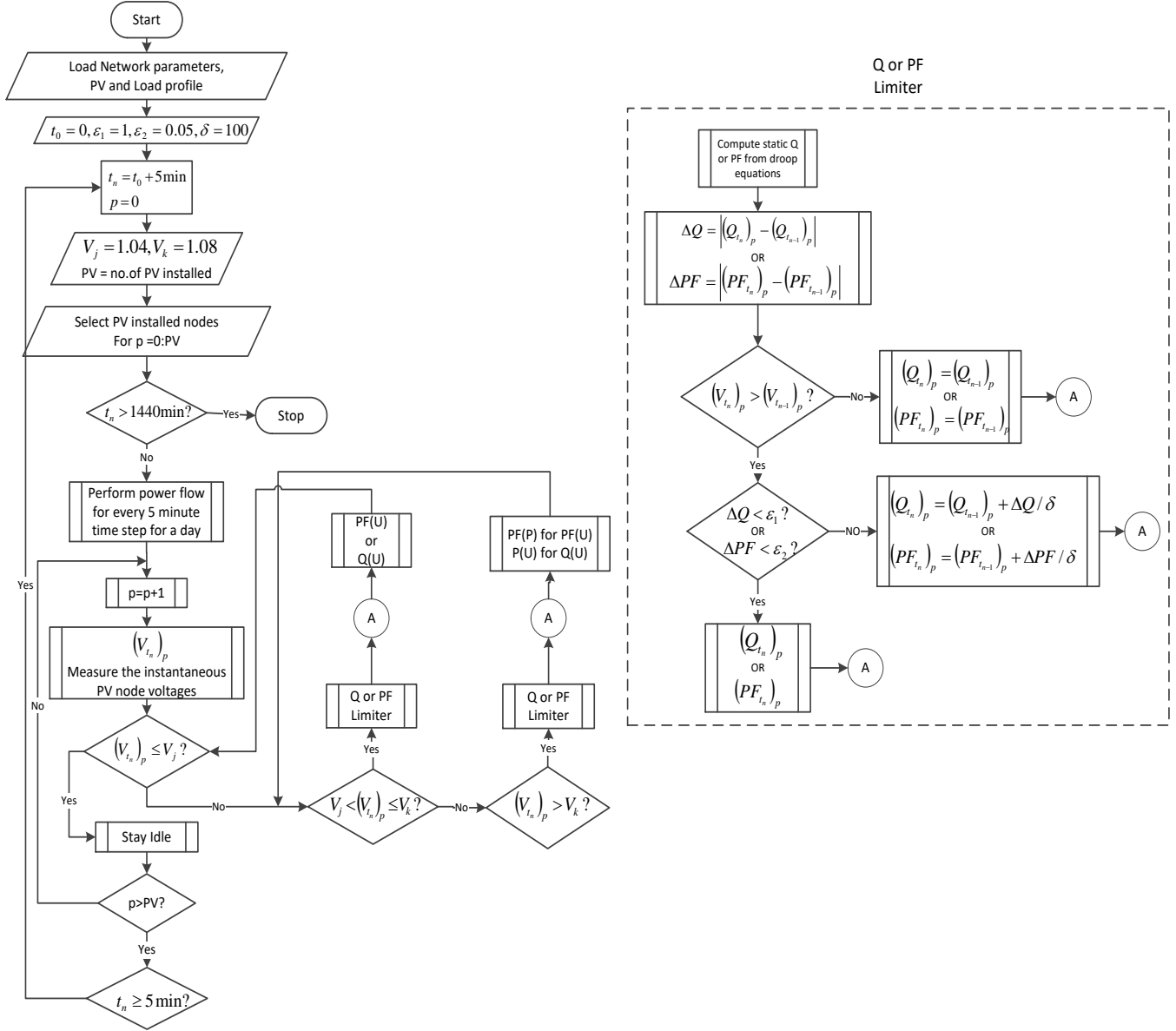
Figure 5: Coordination algorithm

C. Results

With 31 rooftop PVDGs installed out of 74 customers which correspond to 35.65 % of the DT kVA rating, voltage fluctuation as shown in Figure 6 remains within the allowable limit which is ±10% of the nominal value. Herein, the voltage rise is visible starting from node 58 to node 73 from the heat bar (Refer to Appendix 2 Figure A1).
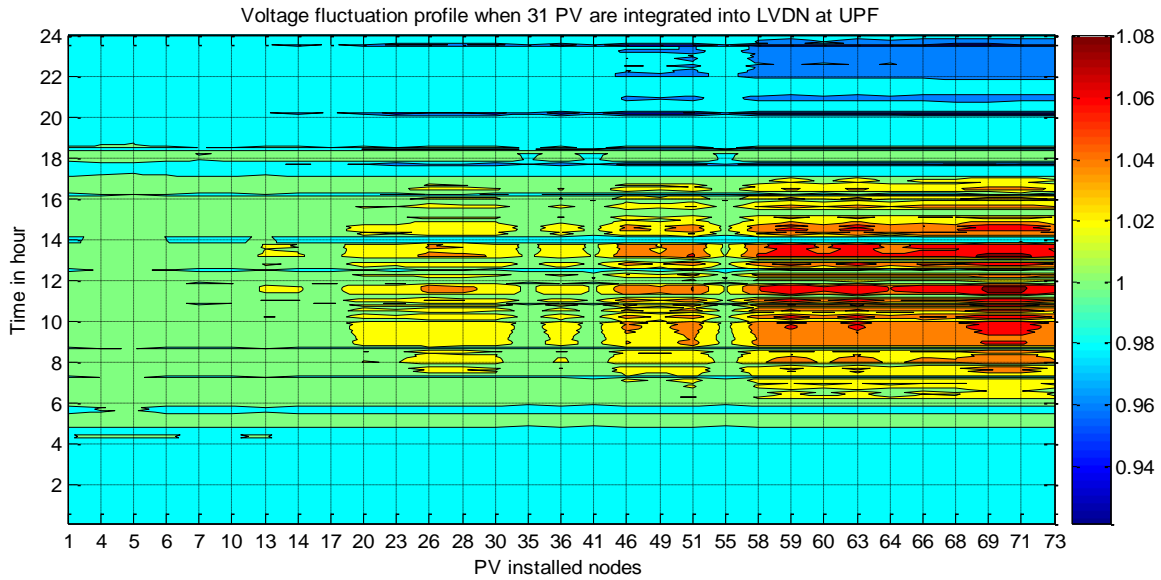
Figure 6: Contour plot Voltage fluctuation profile in each 31 PVDG installed nodes

Whereas, when 58 rooftop PVDGs are installed out of 74 customers corresponding to 66.70% of the DT kVA rating, overvoltage fluctuation (i.e. the voltage at the far end exceeds +10% of the nominal value) occurs at the far end of the feeder, which is shown in Figure 7. Moreover, voltage rise is visible starting from node 55 to node 73 from the heat bar (Refer to Appendix 2 Figure A2).
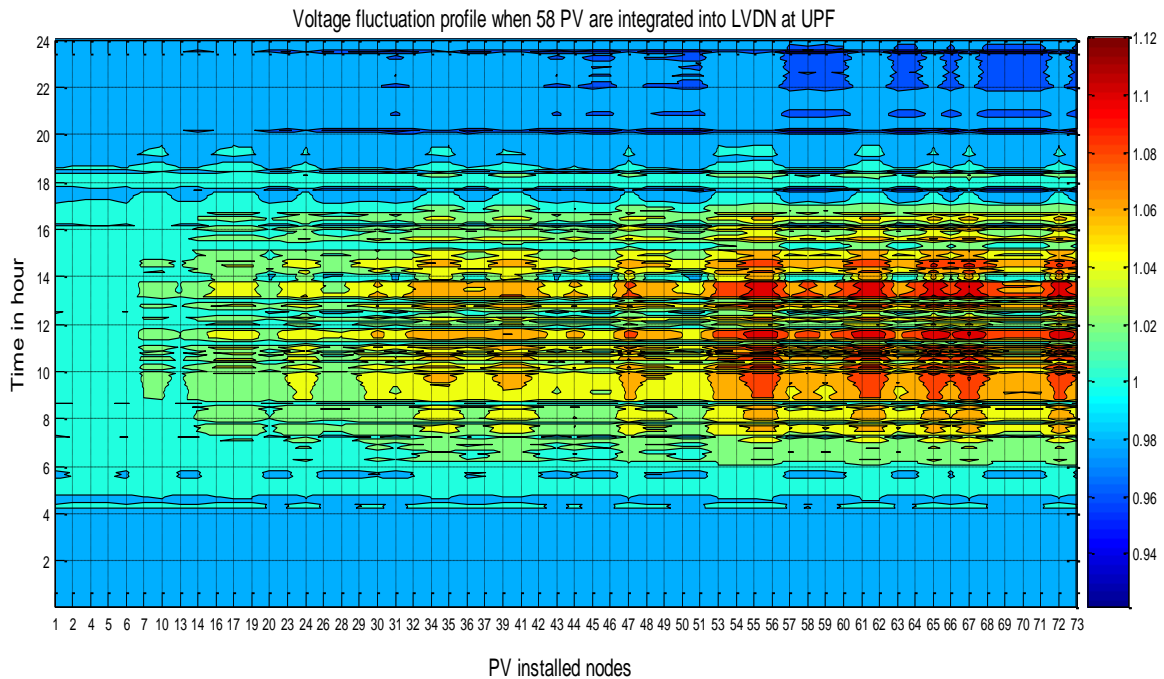

Figure 7: Contour plot for Voltage fluctuation profile in each 58 PVDG installed nodes

From Figure 7, over voltage fluctuations in the LVDN can be observed due to the increased penetration of PVDG installations from 31 to 58 PVDGs at UPF which corresponds to an increase from to 35.65 % to 66.70% of the DT rated kVA. As a consequence of this increase, the last customer node 74th voltage profile is affected by overvoltage

15

exceeding the +10 % of nominal value. Three phase voltages and angles (V_a, V_b and V_c) obtained from the pillar J (see Figure 2) are used to compute the symmetrical components (V^0(zero), V^+(positive) and V^-(negative)) from which, the voltage unbalance factor can be evaluated. The computation process is expressed by Equation (1).

$$\begin{bmatrix} V^0 \\ V^+ \\ V^- \end{bmatrix} = A^{-1} \begin{bmatrix} V_a \\ V_b \\ V_c \end{bmatrix} = \frac{1}{3} \begin{bmatrix} 1 & 1 & 1 \\ 1 & a & a^2 \\ 1 & a^2 & a \end{bmatrix} \begin{bmatrix} V_a \\ V_b \\ V_c \end{bmatrix} \tag{1}$$

The voltage unbalances factor at node J is calculated using Equation (2).

$$\text{Voltage unbalanced factor, } VUF = \frac{V^-}{V^+} \tag{2}$$

Herein, with 58 PVDGs installation at UPF, Figure 8 shows that the statistical variation in the voltage unbalance where the frequency of occurrence is shown for various levels of unbalance. Typically, the standard level requirement is that the unbalance is less than 2% for 95% of a defined period (typically one week). It can be seen that the standard is met in this case.
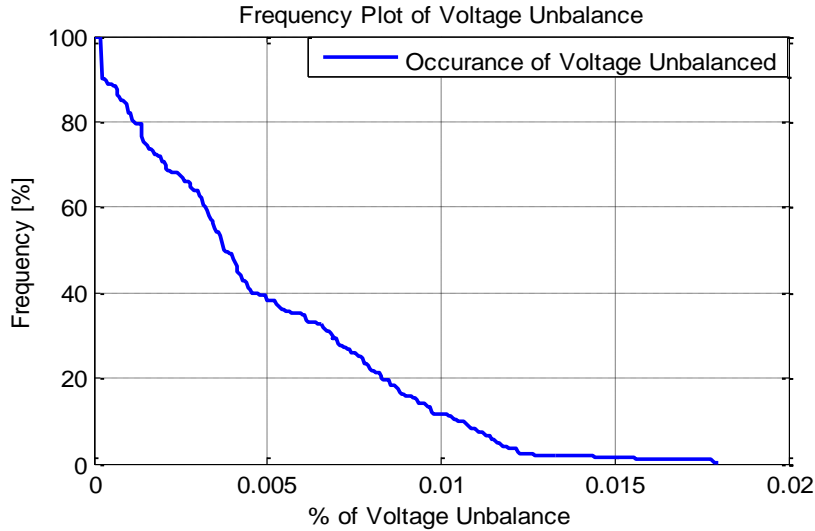

Figure 8: Frequency vs % of Voltage unbalances at pillar J

Hence, in this paper, only voltage fluctuation management will be considered since the entire LVDN is balanced after conglomeration integration of 58 PVDGs and 74 loads. In the following part of this section, the application of different RPCs and two coordinating algorithms for voltage management are discussed followed by the amount of reactive power exchanges in each technique. Figure 9 shows the boxplot of three voltage profiles namely 1st, 73rd and 74th nodes (designated by (a), (b) and (c)) under different techniques namely UPF, Q (U), PF (P), PF (U), Q(U) & P(U) and PF(U) & PF(P). As shown, when all GTIs are embedded with UPF, 73rd and 74th nodes exceed the overvoltage limitation which is +10 % of nominal value. In such a situation, the number of PVDG installations upstream, the far end node, i.e. node 74th, is affected severely without any PVDG installation at its premises. Managing voltage under increased penetration of PVDGs thus becomes an important aspect for all the PV GTIs to alleviate any the voltage fluctuation in the LVDN.
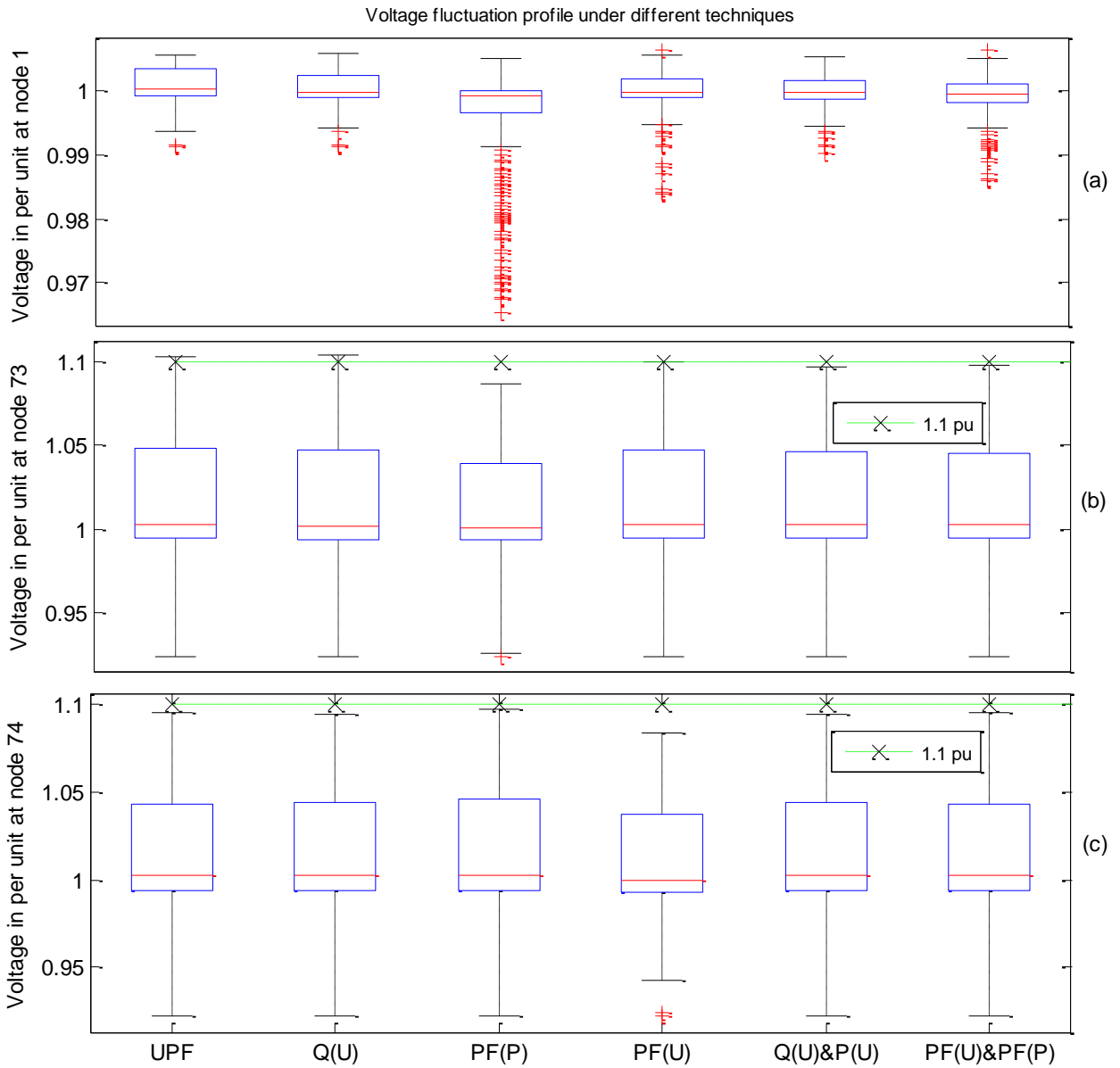
Figure 9: Boxplot of voltage fluctuation profile at nodes (a) 1 (b) 73 and (c) 74 under different techniques when 58 PVDG are installed in LVDN

From Figure 9, when different RPCs are embedded in each of the PV GTIs, it can be seen that voltage management controllability is insufficient and inefficient. For an instance, with Q (U) and PF (U) alone, voltage management is insufficient as both nodes 73 and 74 nearly exceed 1.1 p.u even after utilizing the maximum available kVAr from each GTI as shown in Figure10 (b) for node 73. Referring to PF (P) technique, over voltage is alleviated in both nodes 73 and 74 with higher voltage fluctuation at node 1 when compared to UPF. The reason for such uneven voltage management is due to its controlling technique of PF (P) where the PF is regulated as a function of PV active power. The consequences for PF (P) technique is that irrespective of the instantaneous node voltage, all the PV GTIs will regulate its PF in which reactive power exchange is the same for all the PVDG installed nodes. Such phenomena can

be observed in Figure 10 (a) and (b) at nodes 1 and 73 respectively where an equal amount of reactive power is exchanged for PF (P) techniques.
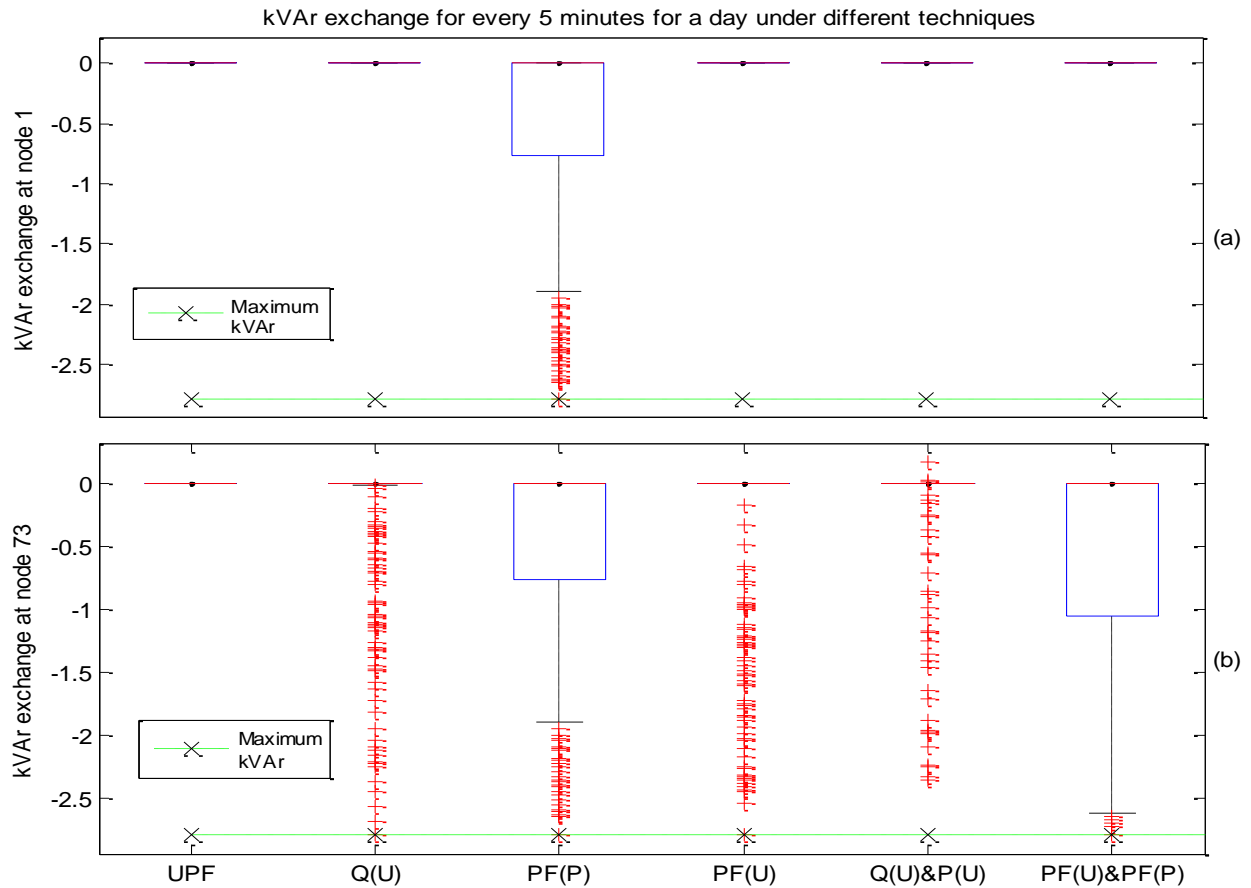

Figure 10: Boxplot of the amount of reactive power exchange **for every 5 minutes for entire day** at nodes (a) 1 and (b) **73** under different techniques when 58 PVDG are installed in LVDN

To overcome each individual controllability limitations of RPCs, the two coordination algorithms namely Q(U) & P(U)and PF(U) & PF(P) shows significant improvement in managing the voltage in all the nodes evenly as shown in Figure 9. Furthermore, PF (U) & PF (P) and Q (U) & P (U) introduce less voltage fluctuation at node 1 as compared with PF (U) and PF (U). As shown in Figure 10 (a) except PF (P) technique, all other techniques don't exchange any reactive power as the voltage at node 1 is under the limit which is illustrated in Figure 9 (a). Whereas, in Figure 10 (b), except UPF technique, all other techniques exchange reactive power to combat the voltage fluctuation at node 73 which is illustrated in Figure 9 (b). It can be observed from Figure 10 (b), with co-ordinating algorithm techniques, the amount of reactive power is optimally utilized to combat any overvoltage violation at node 73. In terms of reactive power exchange, Q (U) & P (U) absorb least amount of reactive power (with no reactive power exchange in most cases) as compared with other techniques in combating the voltage fluctuation which is shown in Figure 10 (b).

Table IV shows average reactive and active power exchange for one day at node 73 under different techniques. Among RPCs, PF (P) absorbs highest average reactive power which is about 0.47 kVAr for the whole day. The two coordinating algorithms namely, PF (U) & PF (P) and Q (U) & P (U) absorb fairly same average reactive power as compared with Q (U) and PF (U). However, in Q (U) & P (U) technique, a small average amount of active power is curtailed which is almost negligible. With respect to voltage alleviation, PF (U) & PF(P) and Q(U) & P(U) is similar as it can be seen in Figure 9 (b) and (c).

TABLE IV

AVERAGE REACTIVE AND ACTIVE POWER EXCHANGE FOR A DAY AT NODE 73 UNDER DIFFERENT TECHNIQUES

Techniques	UPF	Q(U)	PF(P)	PF(U)	Q(U) & P(U)	PF(U) & PF(P)
kVAr absorbed/day	0	0.30	0.47	0.35	0.23	0.23
kVAr exported/day	0	0	0	0	0.002	0
kW curtailed/day	0	0	0	0	0.018	0

Figure 11 shows the demonstration of voltage fluctuation management at node 73 through the proposed two coordinating algorithms. Here, instantaneous PV installed node voltage is continuously measured and appropriately the control actions are taken as described in Section III *B*. It can be observed from Figure 11 that the proposed two coordinating algorithms not only alleviate the overvoltage but also try to smoothen and stabilize the voltage.
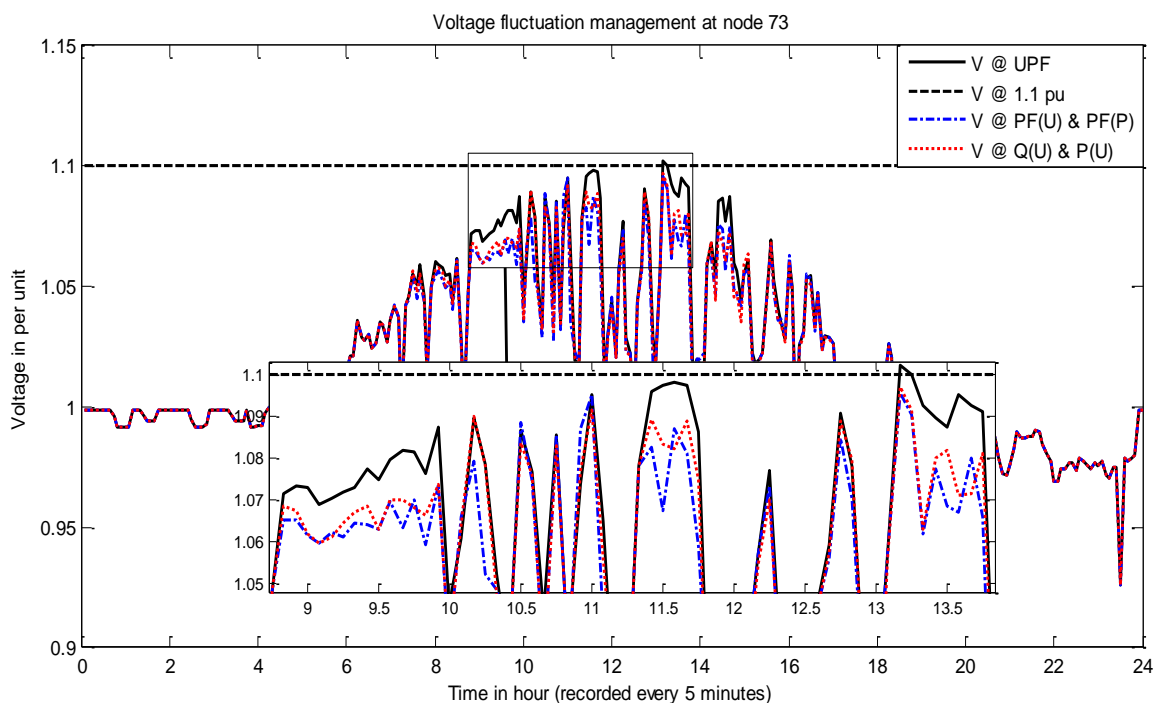

Figure 11: Demonstration of voltage fluctuation management through two coordination algorithm

IV. COMPARATIVE ANALYSIS

In the following part of this paper, comparative analyses of all the different techniques are presented. Table V presents a performance summary on different techniques when 58 PVDGs are integrated into LVDN.

TABLE V

PERFORMANCE TABLE OF ALL THE TECHNIQUES

Techniques applied under 58 rooftop PVDGs penetration	Average losses (CL) for a day CL=(Line +Transformer) losses		Average transformer loading for a day		Average reactive and active power exchange for a day at node 73			Voltage at Node 73 in pu	Voltage at Node 74 in pu
	kW	kVAr	In kVA	In % of DT	kVAr absorb/day	kVAr export/day	kW curtail/day		
UPF	3.90	3.74	85.02	59.78	0	0	0	1.102	1.099
Q(U)	4.03	3.81	85.47	59.61	0.30	0	0	1.103	1.100
PF(P)	4.55	4.43	89.60	65.00	0.47	0	0	1.086	1.083
PF(U)	4.09	3.85	85.57	59.63	0.35	0	0	1.100	1.097
Q(U) & P(U)	3.89	3.72	84.58	59.64	0.23	0.002	0.018	1.097	1.094
PF(U)& PF(P)	4.19	3.93	86.00	60.10	0.23	0	0	1.097	1.095

As presented in Table V, PF (P) maintains the over voltage fluctuation at a cost of high average circuit losses and transformer loading for a day, whereas Q (U) and PF (U) show an inability to alleviate the over voltage. On the other hand, coordinating algorithm Q (U) & P (U) maintain the over voltage and least transformer loading at a cost of curtailing an average active power of 0.018 kW per day. In terms of voltage management, the two proposed algorithms Q (U) & P (U) and PF (U) & PF (P) manage to stabilise each and every PV installed node voltage under the limit. In contrast to the controllability of effective voltage management, circuit losses, and transformer loading; Q (U) & P (U)and PF (U) & PF (P) techniques show significant improvement where PF (U) & PF (P) imposes higher circuit and transformer losses as compared to Q (U) & P(U).
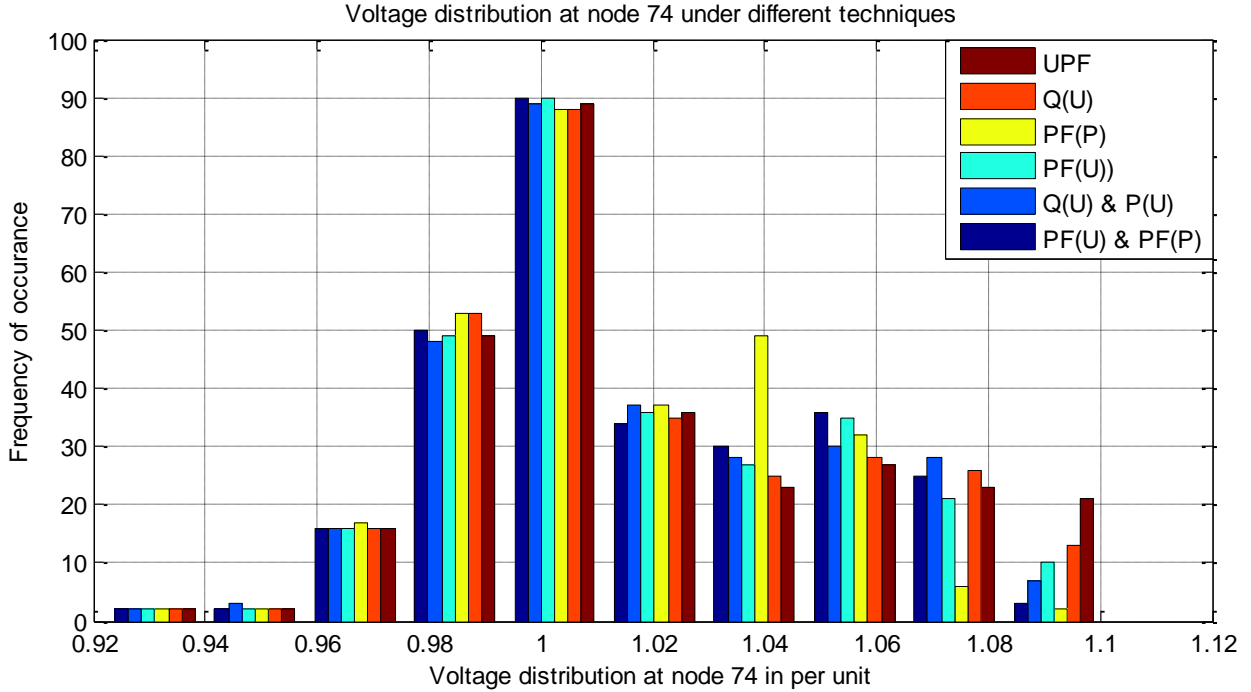
Figure 12: Voltage distribution for node 74 under different techniques

Voltage fluctuation distribution at node 74, where PVDG is not installed in its premises, is shown in Figure 12. Referring to Figure12, almost 90% of all the techniques export electricity at 1 p.u but with UPF operation the voltage fluctuation reaches up to 1.1p.u for almost above 20 % time. In terms of the voltage distribution profile PF (P) shows significant improvement in maintaining the voltage within the limit at node 74 followed by Q (U) & P(U)and PF(U) & PF(P). Both PF (U) and Q (U) techniques show inadequacy in maintaining the voltage within the limit where almost above 10% of the voltage fluctuates within the critical limit. However, with respect to circuit losses and transformer loading, Q (U) & P (U) is one of the best voltage management techniques where it maintains and stabilises the voltage below the critical limit with the negligible amount of active power curtailment.

V. CONCLUSION

With increasing proliferation of rooftop PVDG installations in LVDN, a prevalence of overvoltage phenomena is inevitable. However, by regulating the 2nd and 3rd quadrants of active and reactive GTI power, voltage management can be achieved by optimally controlling the active and reactive power flow from the PVDG sources. This paper focused on coordinating all the PVDG GTIs in a representative LVDN where each PVDG GTI is controlled to limit over-voltage through RPCs alone or through a combination of RPC in conjunction with APC. Moreover, the paper proposed a novel '*Q*' or '*PF*' limiter which restricts frequent switching between the two droop characteristics while ensuring a stabilizing (smoothened) voltage profile in each of the PV installed nodes. From the results and comparative studies, it is evident that RPCs alone are insufficient and inefficient in maintaining voltage within the (*EN 50438*) limit. Moreover, RPCs fail to maintain the voltage profile within the limit at the downstream of the LVDN where PVDG is not even installed; node 74 in this case. The results and comparative studies presented here show that a co-

ordination of Q (U) & P (U) provides higher compliance of allowable voltage regulation level. It also significantly facilitates to increase the PVDG penetration level from 35.65 % to 66.7% of DT kVA rating. Further, it can be seen from the histogram of the very farthest node in the network (node 74, Figure 12) that Q (U) & P (U) is one of the best voltage management technique where it maintains and stabilises the voltage below the critical limit with the negligible amount of active power curtailment. On the other hand, PF (U) & PF (P) impose higher circuit losses and transformer loading as compared to that of Q (U) & P (U) (see Table V).

With this understanding, the future work will investigate the performance of such coordinating techniques under different solar irradiation and customer load profiles from each PV GTI and its aggregate effects on the sub-transmission network when such coordinating algorithms are exploited.

REFERENCES

[1] M. Liserre, T. Sauter and J. Y. Hung, "Future energy systems : Integrating renewable energy sources into the smart power grid through industrial electronics," *IEEE Industrial Electronics Magazine,* vol. 4, no. 1, pp. 18-37, 2010.

[2] F. Katiraei and J. R. Aguero, "Solar PV integration Challenges," *IEEE Power & Energy Magazine,* pp. 62-71, May-June 2011.

[3] G. Spagnuolo and e. al., "Renewable energy operation and conversion schemes: A summary of discussions during the seminar on renewable energy systems," *IEEE Industrial Electronics Magazine,* vol. 4, no. 1, pp. 38-51, 2010.

[4] T. Stetz, F. Marten and M. Braun, "Improved Low Voltage Grid-Integration of Photovoltaic Systems in Germany," *IEEE Transactions on Sustainable Energy,* vol. 4, no. 2, pp. 534-542, 2013.

[5] A. Cagnano, E. D. Tuglie, M. Liserre and R. A. Mastromauro, "Online Optimal Reactive Power Control Strategy of PV inverters," *IEEE Transactions on Industrial Electronics,* vol. 58, no. 10, pp. 4549-4558, 2011.

[6] R. C. Dugan, M. F. McGranaghan,, S. Santoso and H. W. Beaty, Electric Power Systems Quality, 2nd ed., McGraw-Hill, 2002.

[7] M. M. Begovic, I. Kim, D. Novosel, J. R. Aguero and A. Rohatgi, "Integration of Photovoltaic Distributed Generation in the Power Distribution Grid," in *45th Hawaii International Conference on System Science*, Hawaii, 2012.

[8] R. Shah, N. Mithulananthan, R. C. Bansal and V. K. Ramachandaramurthy, "A review of key power system stability challenges for large-scale PV integration," *Renewable and Sustainable Energy Reviews,* vol. 41, pp. 1423-1436, 2015.

[9] J. E. Quiroz, J. M. Reno and R. J. Broderick, "Time Series Simulation of Voltage Regulation Device Control Modes," in *Photovoltaic Specialists Conference*, June 2013.

[10] H. Mortazavi, H. Mehrjerdi, M. Saad, S. Lefebvre, D. Asber and L. Lenoir, "A Monitoring Technique for Reversed Power Flow Detection With High PV Penetration Level," *IEEE Transactions on Smart Grid,* vol. 6, no. 5, pp. 2221 - 2232, August 2015.

[11] M. J. Reno, R. J. Broderick and S. Grijalva, "Smart Inverter Capabilities for Mitigating Over-Voltage on Distribution Systems with High Penetrations of PV," in *Photovoltaic Specialists Conference*, 2013.

[12] P. Y. Agalgaonkar, B. C. Pal and R. A. Jabr, "Impact of PV Generation on Tap Changers," *IEEE Transaction on Power Systems,* vol. 29, no. 1, pp. 182-192, 2014.

[13] J. Jung, A. Onen, R. Arghandeh and R. P. Broadwater, "Coordinated control of automated devices and photovoltaic generators for voltage rise mitigation in power distribution circuits," *Renewable Energy,* vol. 66, pp. 532-540, 2014.

[14] W. Zhang, M. Baran,, A. De and S. Bhattacharya, "Fast Volt–VAR Control on PV Dominated Distribution Systems," in *T&D Conference and Exposition*, 2014.

[15] V. Calderaro, G. Conio, V. Galdi, G. Massa and A. Piccolo, "Optimal decentralized voltage control for distribution systems with inverter-based distributed generators," *IEEE Transanctions on Power systems,* vol. 29, no. 1, pp. 230-241, 2014.

[16] C. H. Chang, Y. H. Lin, Y. M. Chen and Y. R. Chang, "Simplified Reactive Power Control for Single-Phase Grid-Connected Photovoltaic Inverters," *IEEE Transactions on Industrial Electronics `,* vol. 61, no. 5, pp. 2286-2296, 2014.

[17] BDEW, "Technical Conditions for Connection to the medium-voltage network," 2008.

[18] VDE, "Technical minimum requirements for the connection to and parallel operation with low voltage distribution networks," 2011.

[19] E. Demirok, P. C. Gonzalez, K. H. Frederiksen, D. Sera, P. Rodriguez and R. Teodorescu, "Local Reactive Power Control Methods for Overvoltage prevention of Distributed Solar Inverters in Low-Voltage Grids," *IEEE Journal of Photovoltaics,* vol. 1, no. 2, pp. 174-182, 2011.

[20] L. Collins and J. K. Ward, "Real and reactive power control of distributed PV inverters for overvoltage prevention and increased renewable generation hosting capacity," *Renewable Energy,* vol. 81, pp. 464-471, 2015.

[21] X. Liu, M. A. Cramer and Y. Liao, "Reactive-Power Control of Photovoltaic Inverters for Mitigation of Short-Term Distribution-System Voltage Variability," in *T&D Conference and Exposition*, 2014.

[22] S. Weckx, C. Gonzalez and J. Driesen, "Combined Central and Local Active and Reactive Power Control of PV Inverters," *IEEE Transcation on Sustainable Energy,* vol. 5, no. 3, pp. 776-784, 2014.

[23] R. Caldon,, M. Coppo and R. Turri, "Distributed voltage control strategy for LV networks withinverter-interfaced generators," *Electric Power Systems Research,* vol. 107, pp. 85-92, 2014.

[24] P. Jahangiri and D. C. Aliprantis, "Distributed Volt/VAr Control by PV Inverters," *IEEE Transaction on Power System,* vol. 28, no. 3, pp. 3429-3439, 2013.

[25] F. Andrén, B. Bletterie, S. Kadam, P. Kotsampopoulos and C. Bucher, "Distribution Networks With a High Penetration of Inverter-Based Generation," *IEEE Transactions on Industrial Electronics,* vol. 62, no. 4, pp. 2519-2529, 2015.

[26] J. H. Braslavsky, J. K. Ward and L. Collins, "A stability vulnerability in the interaction between Volt-VAR and Volt-Watt response functions for smart inverters," in *IEEE Conference on Control Applications*, Sydney, Australia, 2015.

[27] S. Liu, P. X. Liu and X. Wang, "Stochastic Small-Signal Stability Analysis of Grid-Connected Photovoltaic Systems," *IEEE Transactions on Industrial Electronics,* vol. 63, no. 2, pp. 1027-1038, 2016.

[28] S. B. Kjær, "Grid Voltage Control by PF (U) Regulation," in *29th European Photovoltaic Solar Energy Conference and Exhibition*, Amsterdam, 2014.

[29] A. Samadi, R. Eriksson, L. Söder, B. G. Rawn and J. C. Boemer, "Coordinated Active Power-Dependent Voltage Regulation in Distribution Grids With PV Systems," *IEEE Transactions on Power Systems,* vol. 29, no. 3, pp. 1454-1464, 2014.

[30] E. Serban, M. Ordonez and C. Pondiche, "Voltage and Frequency Grid Support Strategies Beyond Standards," *IEEE Transaction on Power Electronics,* vol. pp, no. 99, 2016.

[31] K. Sunderland, M. Coppo, M. Conlon and R. Turri, "A correction current injection method for power flow analysis ofunbalanced multiple-grounded 4-wire distribution networks," *Electric Power Systems Research,* vol. 132, pp. 30-38, 2016.

[32] SEI, "Your guide to connecting Micro-generation to the Electricity Network," Econnect Ireland, Dublin, 2009.

[33] U. Manchester, "http://www.manchester.ac.uk/," The Whitworth Meteorological Observatory, [Online]. Available: http://www.cas.manchester.ac.uk/restools/whitworth/.

[34] N. A. Espinosa and F. L. Ochoa, "Probabilistic Impact Assessment of Low Carbon Technologies in LV Distribution Systems," *IEEE Transactions on Power Systems*, vol. 31, no. 3, pp. 2192-2203, 2015.

[35] ENWL, "http://www.enwl.co.uk/," Electricity North West, [Online]. Available: http://www.enwl.co.uk/about-us/the-future/lcnf-tier-1-nia/low-voltage-network-solutions.

[36] R. N. Beres, X. Wang, M. Liserre, F. Blaabjerg and C. L. Bak, "A Review of Passive Power Filters for Three-Phase Grid-Connected Voltage-Source Converters," *IEEE Journal of Emerging and Selected Topics in Power Electroncis,* vol. 4, no. 1, pp. 54-69, 2016.

[37] M. Cespedes and J. Sun, "Impedance Modeling and Analysis of Grid-Connected Voltage-Source Converters," *IEEE Transactions on Power Electronics,* vol. 29, no. 3, pp. 1254-1261, 2014.

[38] M. Cespedes and J. Sun, "Mitigation of Inverter-Grid Harmonic Resonance by Narrow-Band Damping," *IEEE Journal of Emerging and Selected Topics in Power Electronics,* vol. 2, no. 4, pp. 1024-1031, 2014.

[39] B. Wen, D. Boroyevich, R. Burgos, P. Mattavelli and Z. Shen, "Analysis of D-Q Small-Signal Impedance of Grid-Tied Inverters," *IEEE Transactions on Power Electronics,* vol. 31, no. 1, pp. 675-687, 2016.

[40] S. Lissandron, L. D. Santa, P. Mattavelli and B. Wen, "Experimental Validation for Impedance-Based Small-Signal Stability Analysis of Single-Phase Interconnected Power Systems With Grid-Feeding Inverters," *IEEE Journal of Emerging and Selected Topics in Power Electronics,* vol. 4, no. 1, pp. 103-115, 2016.

[41] W. Cao, X. Zhang, Y. Ma and F. Wang, "Stability Criterion and Controller Parameters Design of Radial-Line Renewable Systems with Multiple Inverters," in *IEEE Applied Power Electronics Conference and Exposition*, Long Beach, CA, 2016.

[42] P. Channegowda and V. John, "Filter Optimization for Grid Interactive Voltage Source Inverters," *IEEE Transactions on Industrial Electronics,* vol. 57, no. 12, pp. 4106-4114, 2010.

[43] L. Harnefors, X. Wang, A. G. Yepes and F. Blaabjerg, "Passivity-Based Stability Assessment of Grid-Connected VSCs—An Overview," *IEEE Journal of Emerging and Selecteed Topics in Power Electronics,* vol. 4, no. 1, pp. 116-125, 2016.

[44] C. Wan, M. Huang, C. K. Tse and X. Ruan, "Effects of interaction of power converters coupled via power grid: A design-oriented study," *IEEE Transanction on Power Electronics,* vol. 30, no. 7, pp. 3589-3600, 2015.

[45] X. Wang, F. Blaabjerg and W. Wu, "Modeling and Analysis of Harmonic Stability in an AC Power-Electronics-Based Power System," *IEEE Transanction on Power Electronics,* vol. 29, no. 7, pp. 6421-6432, 2014.

[46] Y. Tang, W. Yao, P. C. Loh and F. Blaabjerg, "Design of LCL Filters With LCL Resonance Frequencies Beyond the Nyquist Frequency for Grid-Connected Converters," *IEEE Journal of Emerging and Selected Topics in Power Electronics,* vol. 4, no. 1, pp. 3-14, 2016.

[47] R. D. Middlebrook, "Input filter considerations in design and application of switching regulators," in *IEEE Industry Application Society Annual Meeting*, 1976.

[48] A. G. J.MacFArlane and I. Postlethwaite, "The generalized Nyquist stability criterion and multivariable root loci," *International Journal of Control,* vol. 25, no. 1, pp. 81-127, 1977.

[49] B. Wen, D. Boroyevich, R. Burgos and P. Mattavelli, "Input impedance of voltage source converter with stationary frame linear current regulators and phase-locked loop," in *IEEE Energy Conversion Congress Exposition*, 2013.

[50] Y. Yang, F. Blaabjerg and M. G. Simoes, ""Power control flexibilities for grid-connected multi-functional photovoltaic inverters," *IET Renewable Power Generation,* vol. 10, no. 4, pp. 504-513, 2016.

[51] J. Wang, J. Yan, L. Jiang and J. Zou, "Delay-dependent stability of single-loop controlled grid-connected inverters with LCL filters," *IEEE Transanction on Power Electroics,* vol. 31, no. 1, pp. 743-757, 2016.

[52] C. Yoon, X. Wang, F. F. D. S. Silva, C. L. Bak and F. Blaabjerg, "Harmonic Stability Assessment for Multi-Paralleled, Grid-Connected Inverters," in *IEEE International Power Electronics and Application Conference and Exposition*, 2014.

[53] E. 50438, "www.en-standard.eu," 2007. [Online]. Available: http://www.en-standard.eu/csn-en-50438-requirements-for-the-connection-of-micro-generators-in-parallel-with-public-low-voltage-distribution-networks/.

[54] OpenDSS, "http://smartgrid.epri.com/," Electric Power Research Institute, [Online]. Available: http://smartgrid.epri.com/SimulationTool.aspx.

[55] S. Pukhrem, F. M. Conlon, K. Sunderland and M. Basu, "Analysis of voltage fluctuation and flicker on distribution networks with significant PV installations," in *31st European Photovoltaic Solar Energy Conference and Exhibition*, Hamburg, 2015.

APPENDIX 1

1. To compute the penetration level, the number of PVDG installed and DT kVA rating are essential. Here two types of PVDG integration are performed. In first case 32 PVDG while in second cases 54 PVDG are integrated to the LVDN. The kVA rating of the transformer is 500 kVA and each of the PVDG has the capacity to export 5.75 kW power. In the following calculation of penetration level (PL) in % of DT kVA rating is shown below.

   - PL when there are 31 PVDGs : (31*5.75)/500 % = 35.65%
   - PL when there are 58 PVDGs : (58*5.75)/500 % = 66.70%

2. Source impedance (Zs) calculation:

   Zs = (Voltage at primary side /$\sqrt{3}$)/fault current

     = (per phase value Voltage / fault current) at primary side

     = (20e3/$\sqrt{3}$) / (0.5e3)

     = 23.0940 Ohms

3. Distribution transformer properties include XHL and % loadlosses and their default values are

   XHL = 7%, % load losses =0.4% .Where XHL means percentage of reactance from winding 1 (high) to winding 2 (low) which is expressed in terms kVA base of winding 1. i.e. XHL = 10% of 500 = 50 ohm .

   Here instead of XHL =7%, the author chose XHL=10% in order to include extra 3% reactance losses between winding 1 and winding 2.

   Percentage of load loss is expressed at rated load. By default the %Rs (array of percent resistances for winding 1 and 2) values for windings 1 and 2 are 0.2% and 0.2% respectively. Thus, total transformer %loadlosses=0.4%.

4. Table I summary

   Table A1 summarizes the percentage of the customer with respect to the peak load distribution and PVDGs installation.

Table A1

Peak load distribution in kW	% of customer connecting the load (out of 74)	% of customer installing PVDG (out of 31)	% of customer installing PVDG (out of 58)
$0 < \text{Peak}_{\text{load demand}} < 1$	47.3	48.39%	39.66%
$1 < \text{Peak}_{\text{load demand}} < 6$	33.8	29.03%	37.93%
$\text{Peak}_{\text{load demand}} \geq 6$	18.9	22.58%	22.41%

Here, Table A2 illustrates the percentage of customers consuming different peak load demands at different nodes. About 29 nodes have peak load demand less than 0.5 kW which corresponds to 39.2 % of the total customers. Referring to Table A1, about 47.3 % of total customers has peak load demand ranging in between $0< Peak_{load\ demand}<1$. It is computed by adding 39.2% and 8.1 % from Table A2. Similarly, about 48.39 % of the total PV installed customers i.e. 31 PVDGs has peak load demand ranging in between $0< Peak_{load\ demand}<1$. It is computed by counting the number of PV installed customers having a peak load demand in between $0< Peak_{load\ demand}<1$ from Table A3. Again, about 39.66 % of the total PV installed customers i.e. 58 PVDGs has peak load demand ranging in between $0< Peak_{load\ demand}<1$. It is also computed by counting the number of PV installed customers having a peak load demand in between $0< Peak_{load\ demand}<1$ from Table A3.

Table A2

Peak load demand (P) in kW	Number of nodes	% of total consumers
P<0.5	29	39.2%
0.5<P<1.0	6	8.1%
1.0<P<1.5	0	0.0%
1.5<P<2.0	3	4.1%
2.0<P<2.5	1	1.4%
2.5<P<3.0	5	6.8%
3.0<P<3.5	4	5.4%
3.5<P<4.0	0	0.0%
4.0<P<4.5	2	2.7%
4.5<P<5.0	3	4.1%
5.0<P<5.5	5	6.8%
5.5<P<6.0	2	2.7%
6.0<P<6.5	3	4.1%
6.5<P<7.0	6	8.1%
7.0<P<7.5	5	6.8%
7.5<P<8.0	0	0.0%

Table A3

Node	Load Peak Demand	31 PVDGs	58 PVDGs
1	6.329	5.75	5.75
2	7.198		5.75
3	0		
4	0.294	5.75	5.75
5	0.361	5.75	5.75
6	2.882	5.75	5.75
7	4.459	5.75	5.75
8	0.336		
9	7.214		

10	0.28	5.75	5.75
11	0.467		
12	0.32		
13	0	5.75	5.75
14	0.48	5.75	5.75
15	0		
16	5.387		5.75
17	0.355	5.75	5.75
18	4.339		
19	1.72		5.75
20	5.32	5.75	5.75
21	1.532		
22	3.18		
23	6.925	5.75	5.75
24	0.314		5.75
25	0		
26	3.48	5.75	5.75
27	7.244		
28	0	5.75	5.75
29	6.833		5.75
30	0.518		5.75
31	6.956	5.75	5.75
32	0.66		5.75
33	0.943		
34	4.725		5.75
35	0	5.75	5.75
36	5.064	5.75	5.75
37	0.363		5.75
38	0.314		
39	3.459		5.75
40	0.552		
41	6.315	5.75	5.75
42	0.294		5.75
43	4.837		5.75
44	0.616		5.75
45	5.676		5.75
46	5.419	5.75	5.75
47	0		5.75
48	2.775		5.75
49	5.532	5.75	5.75
50	0		5.75

51	7.216	5.75	5.75
52	0.404		
53	1.966		5.75
54	2.301		5.75
55	2.628	5.75	5.75
56	0.32		5.75
57	3.438		5.75
58	5.095	5.75	5.75
59	4.566	5.75	5.75
60	0.438	5.75	5.75
61	0.41		5.75
62	0		5.75
63	2.773	5.75	5.75
64	6.569	5.75	5.75
65	6.865		5.75
66	0.423	5.75	5.75
67	0		5.75
68	6.444	5.75	5.75
69	7.411	5.75	5.75
70	0		5.75
71	0.562	5.75	5.75
72	0.45		5.75
73	3	5.75	5.75
74	6.916		

Figure A1 illustrates the voltage rise in different nodes. Voltage rise is prominent from node 58 and is highest at nodes 69 and 71. With 31 PVDGs penetration, the voltage rise in all the nodes stays within the limit
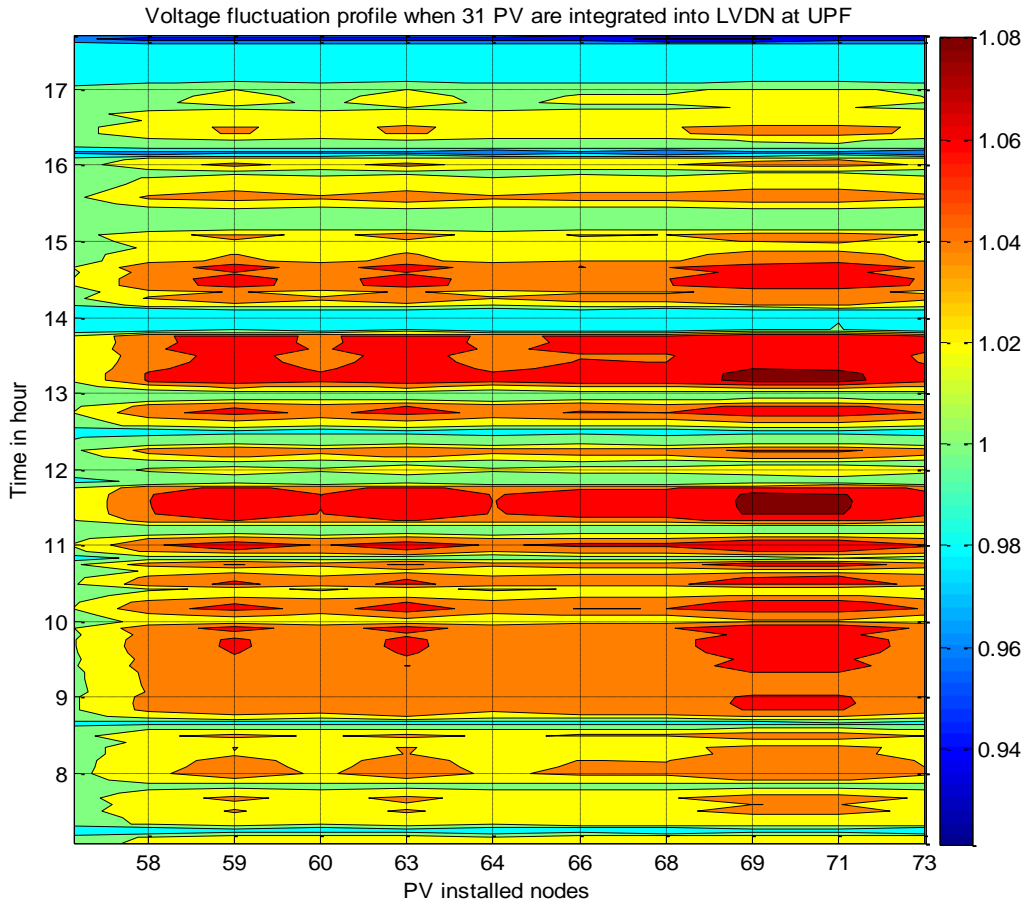

Figure A1: Contour plot Voltage fluctuation profile in each 31 PVDG installed nodes (Zoomed)

Figure A2 illustrates the voltage rise in different nodes. Voltage rise is prominent from node 55 and is highest at nodes 65, 67 and 73. With 58 PVDGs penetration, the voltage rise starts to exceed the limit in nodes 55, 56, 61,62,65,66,67,68,72 and 73.
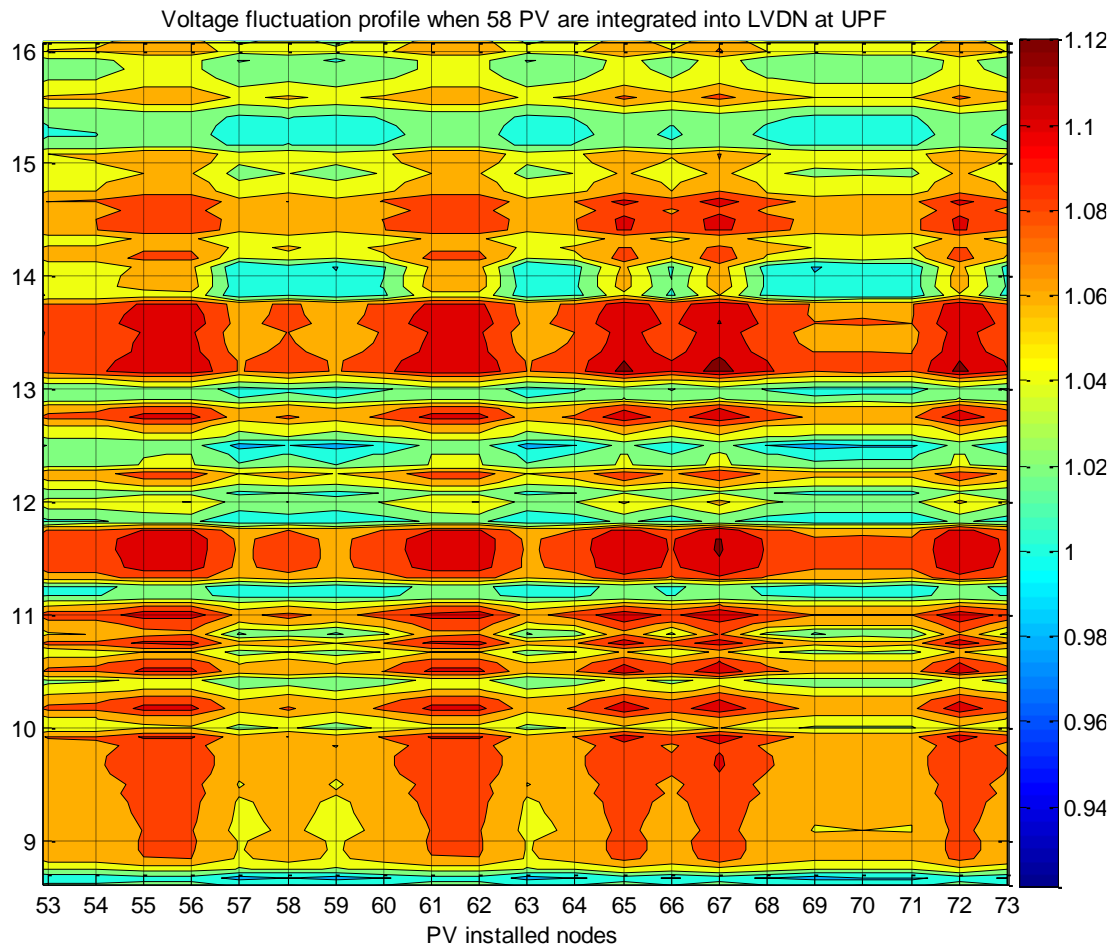
Figure A2: Contour plot Voltage fluctuation profile in each 58 PVDG installed nodes (Zoomed)